OPERATING PRINCIPLE OF SHADOWED C-SI SOLAR CELL IN PV-MODULES

Stefan Wendlandt[1,2], Alexander Drobisch[1], Dirk Tornow[1], Matthias Friedrichs[1], Stefan Krauter[1,3] and Paul Grunow[1]

[1] Photovoltaic Institute Berlin, Berlin, Germany

[2] Department of Energy and Automation Technology, Technical University of Berlin, Berlin, Germany

[3] University of Paderborn, Faculty of Electrical Engineering, Informatics and Mathematics, Electrical Energy Technology - Sustainable Energy Concepts, Paderborn, Germany

1. Abstract

One of the most crucial issues for PV modules is the thermal stability during shading situations. Principally, the hot spot risk can be attributed directly to the properties of the solar cell. The increased hot spot risk at cells results on the one hand from local shunts, deformations of the *p-n*-junction, impurities and the resistance of the raw wafer material and on the other hand from bad cell processing. The risk can be reduced by using shorter solar cell strings and by using advanced in-line quality control tools for cell testing. This work presents the investigation about the operating principle of shadowed solar cells in PV modules. Thereby a focus is the understanding of the current flow in the dark and in the irradiated part of the shadowed cell. Finally, by means of this current examination the dissipated power can be determined.

Keywords: Photovoltaic; Hot Spot; Crystalline silicon cells; Reliability

2. Introduction

PV installation density increases, and more systems suffer from shadowing along with the related hot spot risks. Typical shading situations of PV modules are resulting from antennas, bird droppings, self-shading of adjacent modules, trees, smokestacks and/or from support structures. Basically, each solar cell has a certain hot spot risk which causes (under unfavorable conditions) that the cell's operating point is transferred into reverse voltage and results in heat dissipation. A typical shadowing situation of a standard multi-crystalline PV module and the origin of a hot spot are shown in Figure 1.

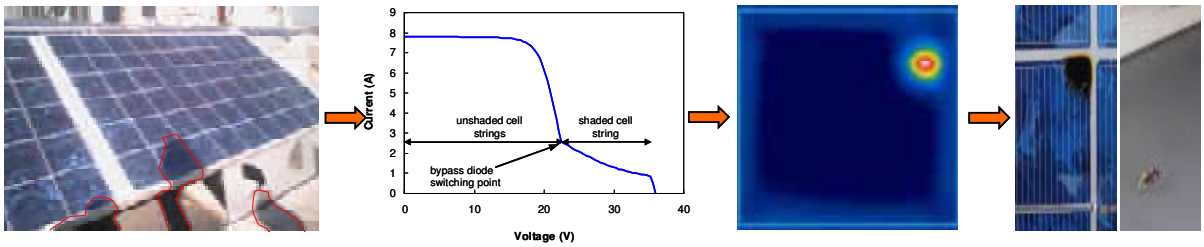

Fig. 1: Origination of a hot spot at a PV module. From left to right: shading a solar cell by building structures (red outline), breakdown of the *IV* curve caused by the shading, local temperature increase of the solar cell by the reverse voltage, thermal destruction of the solar cell, and decomposition of the insulation film on back.

The *IV* reverse bias characteristic of solar cells, its properties and the hot spot phenomena were studied on different ways. In 1934 Zener posited the property concerning the breakdown of electrical insulators (Zener breakdown) [1]. At first in 1954 McKay presented an avalanche theory of breakdown at room temperature [2]. Breitenstein et al. (2010) investigated the junction breakdown in multi-crystalline solar cells [3]. Furthermore Breitenstein et al. (2010) also analysed the influence of defects on solar cell characteristics [4]. Hartman et al. (1980) [5], Spirito and Abergamo (1982) [6], Lopez Pineda (1986) [7], Bishop (1988) [8], Quaschning (1996) [9] and Alonso-García et al. (2006) [10] presented different models of the reverse characteristics of solar cells developed. M. Simon et al. (2010) [11] studied the analysis and detection of hot spots at single cells. The influence of cell texturization on the breakdown has been represented by

Nievendick et al. (2011) [12] and Lausch et al. (2008) [13]. On the pv module site Wohlgemuth (2005) [14] and Herrmann (1997) [15] proposed hot spot test for standards. A hot spot risk factor analysis at PV modules has been carried done by Wendlandt et al. (2010) [16]. In 2010 Pingel [17] showed the influence of the potential induced degradation on the reverse characteristics of solar cells and panels.

3. Experimental set-up & technical description

The tests have been performed on a single-crystalline PV module. The module has 60 solar cells connected in series. Each cell has an edge length of 156 mm x 156 mm. The module is divided into three cell strings. Each string consists of 20 solar cells and one bypass diode. The tests have been performed at the solar cell with the highest leakage current (= bypass diode switching point) in full shading conditions according to the standard IEC 61215-2 Ed. 2 (2005) for standard test conditions.

During the tests the following electrical currents have been measured: the total module current I_{module}, the current through an unshadowed string I_{unsha}, the current through the shadowed string (= shadowed cell) I_{sha}, the current through the bypass diode I_{diode}. In addition, the following voltages have been measured: the voltage of an unshadowed solar cell V_{unsha}, the voltage of the string with the shadowed solar cell V_{string} and the voltage drop of the shadowed solar cell V_{sha}. The measurements have been recorded via calibrated multimeters (max. voltage error: ± 2%, max. current error: ± 2%) and with a logging interval of Δt = 1 sec.

For the experiments a class C (homogeneity class B, class spectrum: C, temporal stability class: B) steady-state solar simulator has been applied. The irradiation unit of the simulator consists of eight metal halide lamps, each with an electronic ballast. For the measurements the steady state solar simulator has been set to an irradiance value of $E_e = (1000 \pm 5)$ W/m² on the plane of module and reached a temperature of $T = (50 \pm 10)$°C on the unshadowed module area under thermally stable conditions.

To realize measurements under different loads of the module an ohmic resistance has been used. The resistance has been connected in parallel to the module terminal.

The hot spot temperature has been measured via an *IR*-camera with an absolute measurement error of ± 2 K, a resolution of 320 x 240 pixels and a thermal sensitivity of 0.1 K at 30 °C. The temperature has been measured on the front glass of the module. During the infrared image recording, the module has been taken off the steady-state solar simulator. During that period the missing irradiation resulted in a cooling of the module, which resulted in a reduction of hot spot temperature of 2 K (absolute). The distance between camera lens and module surface was fixed to 0.66 m. The camera itself has been tilted by 15 degrees from the normal of the module during the measurements. The duration of each measurement has been about 15 minutes - then the module reached thermally stable conditions.

For the hot spot analysis the following shading rates sz = 100.0%, 75.0%, 66.7%, 50.0%, 33.3% and 25.0% have been applied. For each degree of shading, the measurements have been done at the following load points: the *global MPP*, the *local MPP*, the *bypass-diode switching-point* and the others in the following fixed operation points: R = 0 ohms, 1.1 ohms, 4.2 ohms, 9.5 ohms, 125 ohms. For a better understanding of these working points in power-voltage-curves at the different shading rates are shown in Figure 1. In addition to that, the corresponding current-voltage-characteristics are also shown as well.

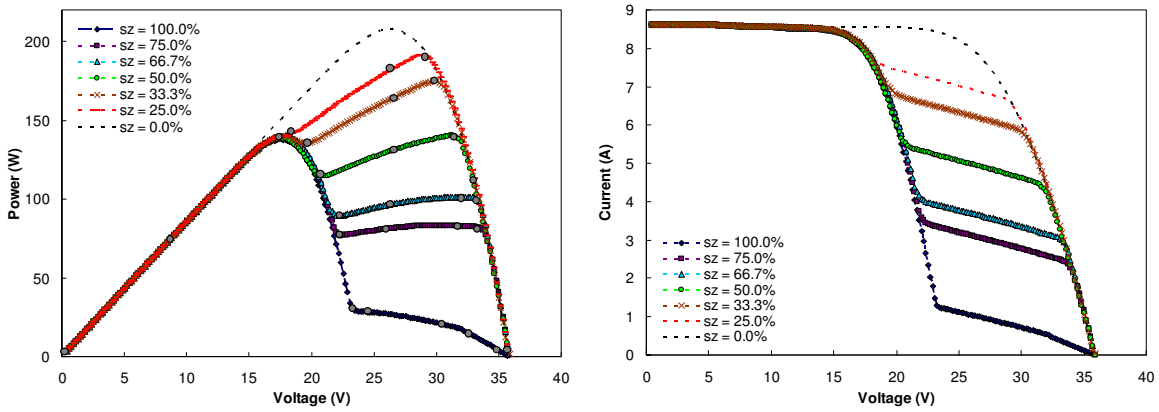

Fig. 1: Power-voltage characteristics (left) with the hot spot analysis of the investigated operating points (gray) and the corresponding current-voltage characteristics (right).

4. Results

Figure 2 shows the voltages and currents measured in different operating points of the module for a cell with shading rates of sz = 100% and 25%. Each measurement has been carried out for a time period of t = 15 min to reach thermal equilibrium.

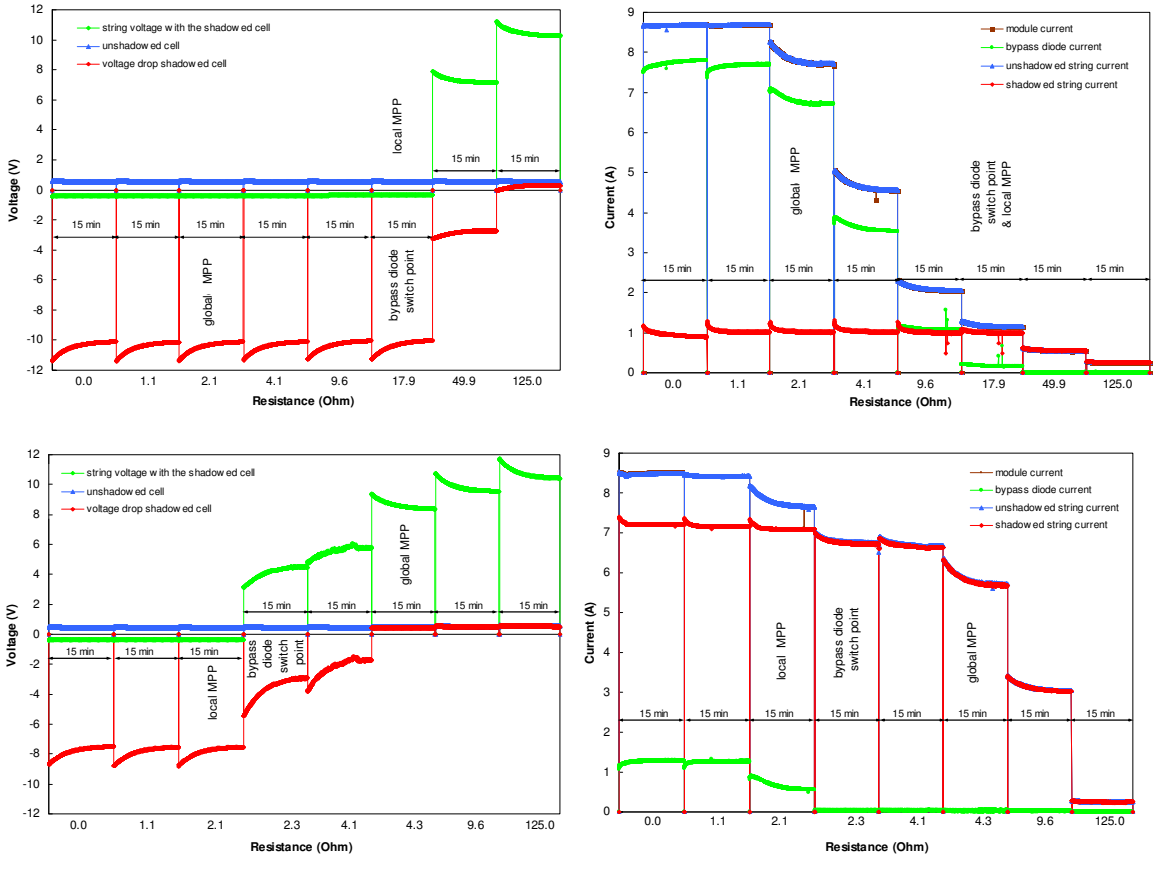

Fig. 2: Measured PV module voltages (left) and currents (right) during the time period from initial state to thermal equilibrium for a cell shaded by 100% (above) and by 25% (below).

Figure 2 shows that the bypass diode switches into "pass" mode, as soon as a module string gets an inhomogeneous radiation. The diode voltage operates in reverse bias in the string loop. The voltage-drop across the shaded solar cell itself depends on the voltage of the unshaded cells in the same string and the number of unshaded cells in the same string, the bypass diode voltage and the degree of shading at the

investigated solar cell. This voltage relation and operating principle is displayed for the initial state in Figure 3. Accordingly, in case of the fully shaded cell a voltage drop of -11.5 V at initial state and -10.1 V at thermally equilibrium can be observed. The voltage reduction itself can be attributed to a negative temperature coefficient of the unshaded solar cell in the same string by heating-up through current flow and irradiation.

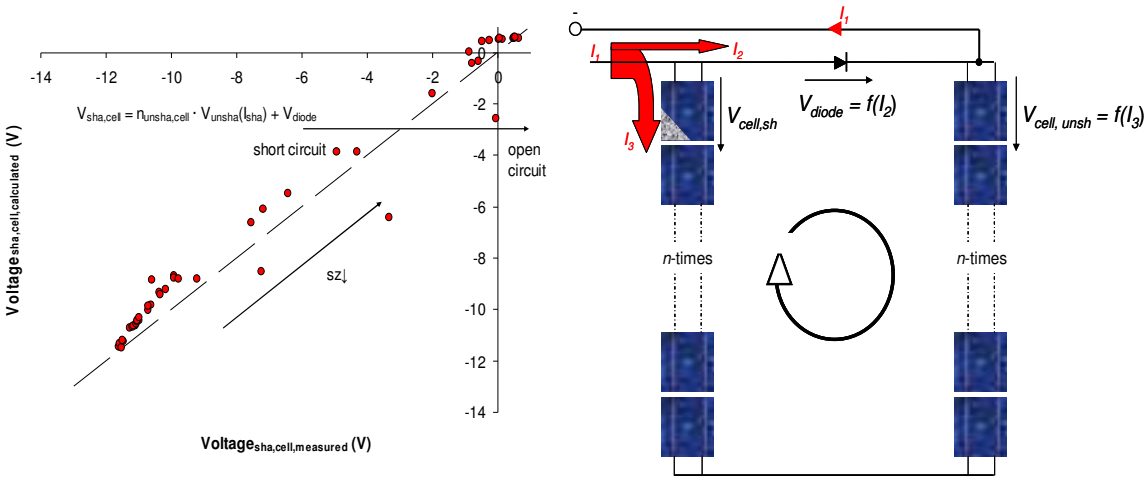

Fig. 3: Comparison of the measured with the calculated voltages at the shadowed solar cell for different loads applied (left). Loop of voltages in a module with a shadowed solar cell in one string (right).

By comparing the measured with the calculated voltage-drop at the shadowed cell, a good correlation among them can be observed. Physically, the voltage in string mash meets Kirchhoff's voltage laws:

$$\sum_{k=1}^{n} V_k = 0 \qquad \text{(eq. 1)}$$

Applying that formula to the string mesh results in:

$$V_{sha,cell} - n_{unsha,cell} \cdot V_{unsha,cell}(I_{sha}) - V_{diode}(I_{diode}) = 0 \qquad \text{(eq. 2)}$$

By interpretation of formula 2 it becomes visible that the voltage drop at the shadowed cell dependents primarily of the number of unshadowed cells in the string mesh.

After explaining the voltage-drop at a shadowed cell, the current-flow through the cell will be discussed. Figure 2 shows that the current is increasing from the case of short circuit to the case of open circuit. The increased current through the bypass diode over time at low module resistances can be explained by a lower diode threshold voltage by the temperature increase. The temporal change of the current at the shadowed string can described in this way. The operating principle of the current in a string with shadowed cell is displayed in figure 4.

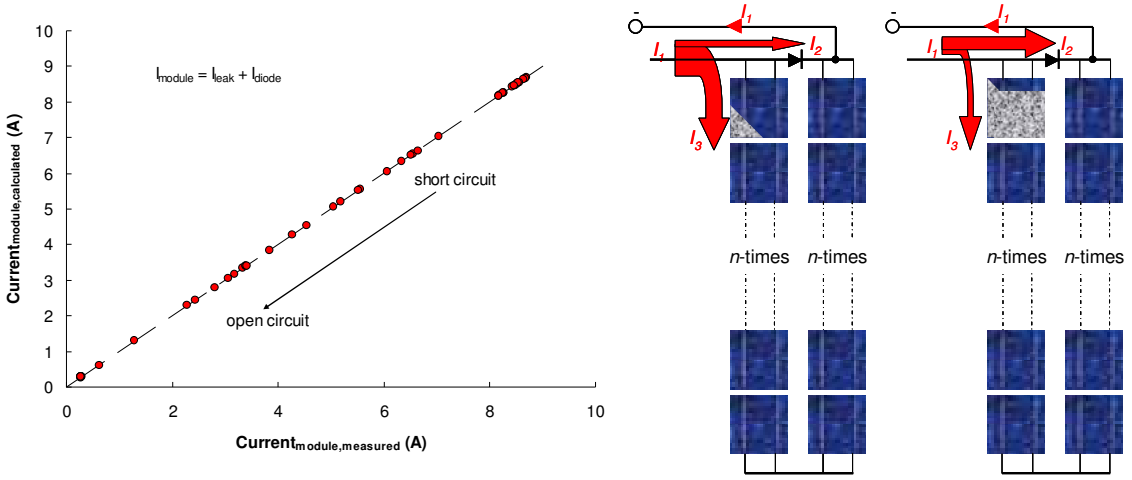

Fig. 4: Comparisons of the measured and calculated currents in the pv module (left) with different loads and shading levels. Balance of currents in a module for different shading levels at a shadowed cell in one string (right).

Also the comparison between the measured and the calculated currents in the string with a shadowed cell shows a fine correlation. That can be traced back to the Kirchhoff's circuit law:

$$I = \sum_{k=1}^{n} I_k \qquad \text{(eq. 3)}$$

By applying that law to a module string it results:

$$I_{\text{module}} = I_{leak}(sz) + I_{diode} \qquad \text{(eq. 4)}$$

Due to figure 4 it becomes clear that the current through the shadowed cell increases by reduction of the shadowing rate. That can be described with that in addition to the leakage current I_{leak} there exists also the photo current I_{ph} through the irradiated part of the cell. To separate both currents in a first step the currents and voltage points of the shadowed cell are fitted by the two-diode model with reverse bias extension term from Quaschning [18].

$$I(V) = I_{ph} - I_{01}\exp\left[\frac{q(V+IR_s)}{kT} - 1\right] - I_{02}\exp\left[\frac{q(V+IR_s)}{kT} - 1\right] - I_{leak} \qquad \text{(eq. 5)}$$

With

$$I_{leak} = \frac{V+IR_s}{R_p} - b(V+IR_s)\left(1 - \frac{V+IR_s}{V_{Br}}\right)^{-n} \qquad \text{(eq. 6)}$$

The measurement points and fits together with the maximum power loss curve of the shadowed cell are shown in figure 5.

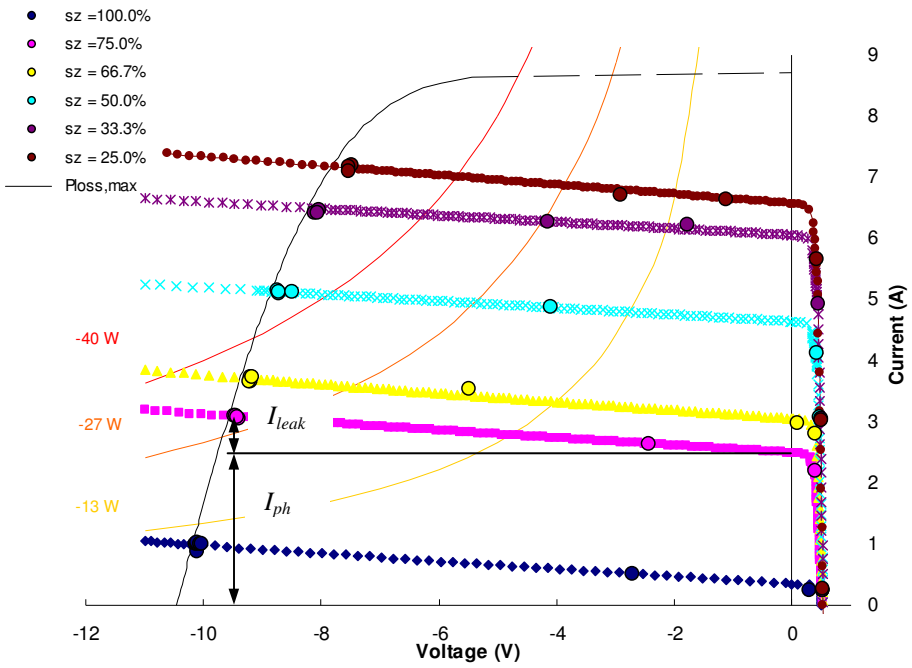

Fig. 5: Measurement points and fits together with the maximum power loss curve of the shadowed cell.

Figure 5 demonstrates that the photo-current increases with smaller shadowing rates. It becomes also clear that with smaller shadowing rates the power loss at the shadowed cell also increased. The difference between measurement points and fitting curves is resulting from measurement errors. The ratio between I_{leak} and I_{ph} as a function of the cell voltage for different shadowing rates is shown in figure 6.

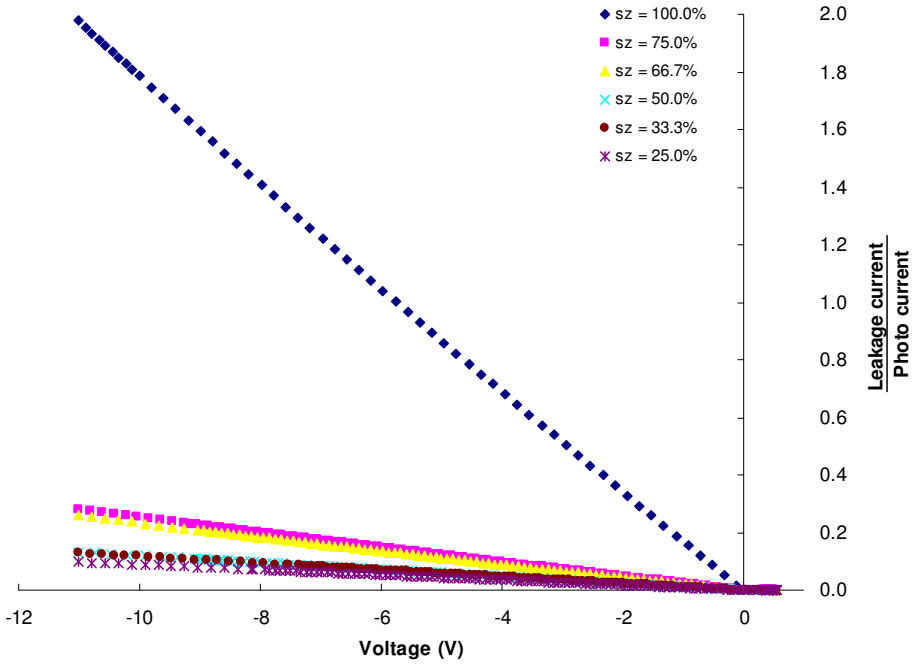

Fig. 6: Relationship between leakage- and photo-current as a function of cell voltage for different shadowing rates.

Figure 6 shows that for a fully shadowed cell the leakage current is the dominating one. In case of partly shadowed situations the photo current becomes dominating. Also the influence of the voltage becomes visible so it can be said that at higher voltages the ratio of leakage-photo currents increases. This is due to the leakage current's influence because the photo current is limited by the irradiated cell area in reverse bias.

Caused by the inhomogeneous properties (specifically the local parallel resistance R_p and the local breakdown voltage V_{br}) of the cell, the leakage current is distributed over the dark and irradiated cell area. For the fully shadowed cell situation it is getting easy to determine the current because it equals to the string current. For situations with partly shadowed cells the separation of the leakage current into the share of dark $I_{leak,1}$ and of light $I_{leak,2}$ is becoming more difficult. Figure 7 shows the scheme of current flows through a partly shadowed cell as described above.

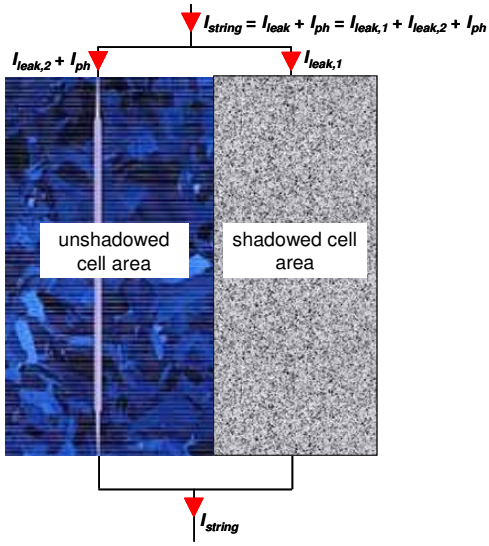

Fig. 7: Balance of current flows through a partly shadowed solar cell.

Therefore the following current model can be established:

$$I_{string} = I_{leak}(R_p, V_{br}) + I_{ph}(sz, E_e) = I_{leak,1}(R_{p1}, V_{br1}) + I_{leak,2}(R_{p2}, V_{br2}) + I_{ph}(sz, E_e) \qquad \text{(eq. 7)}$$

Thereby the photo current is calculated by the current density of the cell at unshadowed conditions and the shadowing rate.

After knowing the reverse voltages and the different currents, the according dissipation powers can be determined. The power curves as a function of the shadowing rate are shown in figure 8.

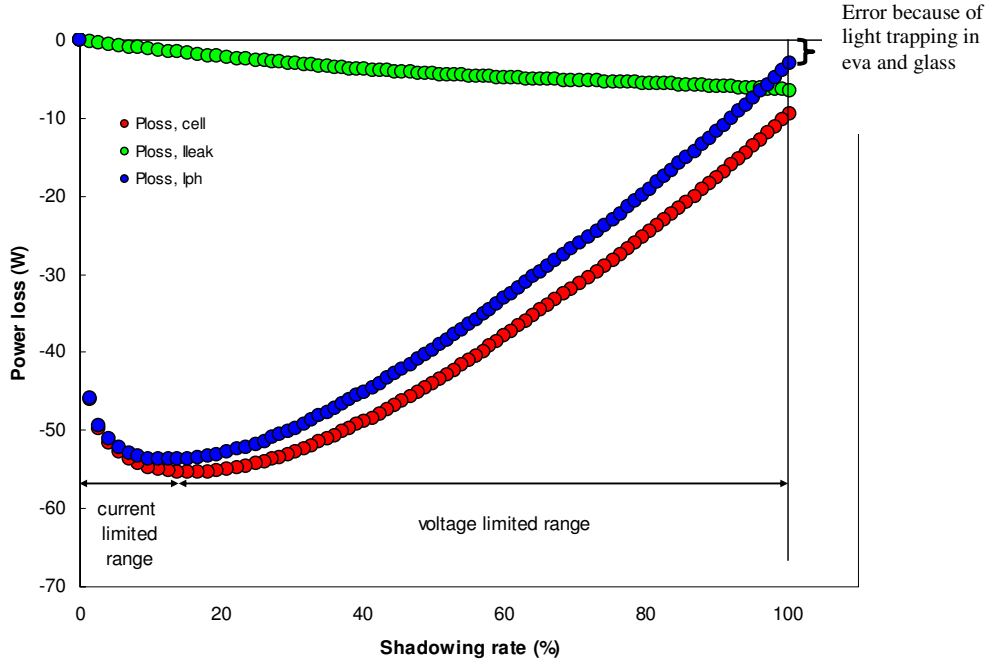

Fig. 8: Dissipation power of shadowed solar cell for different levels of shadowing.

In figure 8 the reduction of the dissipation power for the leakage current at increasing shadowing levels is clearly visible. Also it becomes clear that the total dissipated power is dominated by the photo current. Furthermore, an offset of the dissipation power from the photo current is visible. This is an effect of light trapping in the encapsulation material and the glass above the glass. The total power loss curve (red) itself shows a maximum of dissipation for a shadowing rate of 17%. This point divides the operational status of the shadowed cell into: current (for smaller rates) and voltage (for larger rates) limited ranges.

In figure 7 it is visible that the leakage current is divided into the dark and light part. To determine the partial leakage current of each part the measured means of the temperature distribution in the dark and light part of the shadowed cell and a reference temperature of an unshadowed module range $T_{ref,mean}$ is applied. The leakage currents are calculated by the following model:

$$\frac{I_{leak,2}}{I_{leak,1}} = \frac{T_{2,mean}}{T_{1,mean}} - \frac{T_{ref,mean}}{T_{1,mean}} = \frac{T_{2,mean} - T_{ref,mean}}{T_{1,mean}} \qquad \text{(eq. 8)}$$

Figure 9 shows the leakage currents of each part over the shadowing rates. The currents are determined on the measured temperatures shown in the small window in figure 9 and equation 8.

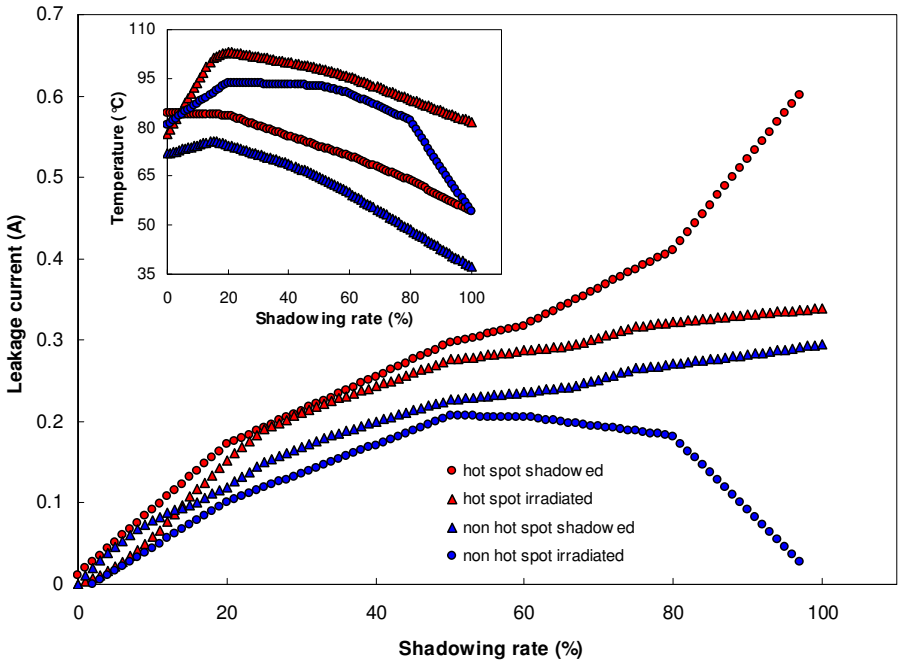

Fig. 9: Leakage current and temperature (small window) over the shadowing rates for a shadowed solar cell.

Figure 9 shows that large shadowing rates cause the highest leakage current. Furthermore it becomes clear that in case of shadowing of the hot spot a higher leakage current flows through the shadowed cell part. That can be due to a less dark resistance of this cell part. In a situation of irradiating the hot spot this cell part also shows a higher leakage current. From there it could be found that the part with the lower leakage current operates as a well blocking diode and the part with the high leakage current as a weak blocking diode.

Finally, the power dissipation for the dark and lighted cell part over the shadowing rates is shown. Figure 10 displays the results.

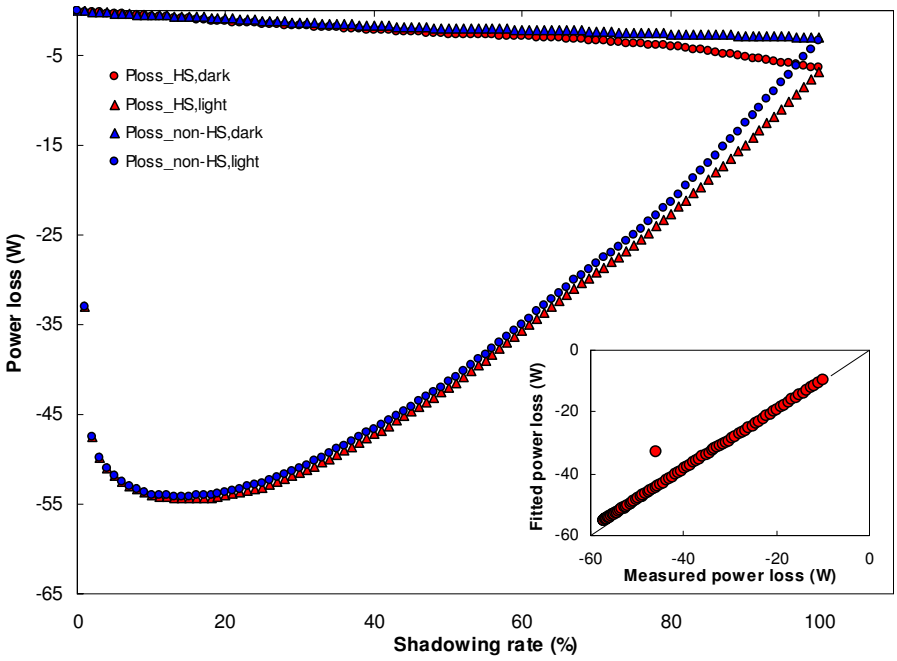

Fig. 10: Power loss of shadowed and unshadowed part over the shadowing rate.

Figure 10 shows the power loss for the case of shadowing and unshadowing the hot spot. For both situations the losses for the dark and lighted part are shown. By interpreting the figure it becomes clear the irradiated cell part shows a higher power loss. That can be due to a strong influence of the photo current on the power loss. Furthermore the figure shows that in case of a lighted hot spot there the highest power becomes dissipated. The small window in figure 10 shows the error between measured power (figure 8) and the modeled power following equation 7.

By comparison of the results in figure 10 and the measured temperatures in figure 9 a well correlation between hot spot temperature and dissipated power is visible. Consequently it was found that a higher hot spot risk for shadowed solar cells exists if the hot spot itself is not shadowed.

5. Conclusions

The hot spot problem depends on the solar cell raw material, the cell process quality and the cell sorting in a module. This paper showed that in case of shadowing a part of a cell this cell operates as a load. This could be due to that the voltage of the shadowed cell becomes negative.

It could be shown that under short current conditions the highest dissipation power drops at a shadowed cell. The level of the dissipation power depends on the reverse bias voltage and the current through the cell. Thereby the reverse bias voltage depends on the number of unshadowed cells in the string mesh and the voltage of the bypass diode. The current consists of two parts, on the one hand the leakage current, which results in the solar cell properties, and on the other hand in the photo current at partly shadowed solar cells. An analyse between both currents had displayed that the relationship-value decreases with smaller shadowing rates, which means that the leakage current becomes decreased and the photo current becomes increased. Furthermore it could be found out that at fully shadowing situations the leakage current shows the highest value. However the photo current has a maximum in the range of smaller shadowing rates.

In this paper a model was applied to separate the global leak current into the dark and the light part. The model is based on the means of the temperature distribution of the dark and lighted part of the shadowed cell. The results showed that the highest leakage current flows through the highest defect range of the cell.

By calculating the power loss for the shadowed and unshadowed part at different shadowing rates it was found that the worst condition exists when the hot spot becomes irradiated.

6. Acknowledgements

The author would like to thank the whole Photovoltaik Institut Berlin team, especially my Ph.D. supervisor Stefan Krauter who sacrificed his whole weekend to finish this paper and Paul Grunow who was reachable his holiday, and of course the Reiner-Lemoine-Foundation for the financial support through a scholarship.

7. References

[1] C. Zener, Proc. Roy. Soc. A145, 523 (1934)

[2] K. G. McKay und K. McAfee, „Avalanche Breakdown in Silicon", Phys. Rev. 94, 877–884 (1954)

[3] O. Breitenstein et al., "Understanding junction breakdown in multicrystalline solar cells", Proceedings 20th Workshop on Crystalline Silicon Solar Cells & Modules, p. 1 - 13 NREL, Breckenridge, USA (2010)

[4] O. Breitenstein et al., "Influence of Defects on Solar Cell Characteristics", Solid State Phenomena Vols. 156-158 (2010) pp 1-10

[5] R.A. Hartman, J.L. Prince, J.W. Lathrop, Second quadrant effect in silicon solar cells, in: Proceedings of the 14th IEEE Photovoltaic Specialists Conference, San Diego, 1980, p. 119–122.

[6] P. Spirito, V. Abergamo, Reverse bias power dissipation of shadowed or faulty cells in different array configurations, in: Proceedings of the Fourth European Photovoltaic Solar Energy Conference, 1982, p. 296–300.

[7] C.F. Lopez Pineda, Solid Wind Technol. 3 (2) (1986) 85.

[8] J. W. Bishop, "Computer simulation of the effects of electrical mismatches in photovoltaic cell interconnection circuits", Solar Cells 25 (1988), p. 73 – 89

[9] V. Quasching, R. Hanitsch, Sol. Energy 56 (6) (1996) 513.

[10] M.C. Alonso-García et al., "Analysis and modelling the reverse characteristic of photovoltaic cells", Solar Energy Materials & Solar Cells 90 (2006), p. 1105-1120

[11] M. Simon et al., "Detection and analysis of hot-spot formation in solar cells", Solar Energy Materials & Solar Cells 94 (2010), p. 106-113

[11] J. Nievendick et al., "Influence of Trench Structures Induced by Texturization on the Breakdown Volatage of Multicrystalline Silicon Solar Cells", Photovoltaic Specialists Conference, 37th IEEE (2011)

[13] D. Lausch et al., Phys. Status Solidi RRL 3, No. 2–3, 70–72 (2009)

[14] J. Wohlgemuth, W. Herrmann, "Hot spot tests for crystalline silicon modules" Photovoltaic Specialists Conference, 31st IEEE (2005), p. 1062

[15] W. Herrmann et al., "Hot spot investigations on PV modules - new concepts for a test standard and consequences for module design with respect to bypass diodes", 26th IEEE Photovoltaic Specialists Conference, Anaheim (1997), p. 1129-1132

[16] S. Wendlandt, A. Drobisch, T. Buseth, S. Krauter, P. Grunow, "Hot spot Risk analysis on silicon cell modules", 25th European Photovoltaic Solar Energy Conference, Valencia, Spain, 2010

[17] S. Pingel et al., "Potential Induced Degradation of solar cells and panels", 35th IEEE Photovoltaic Specialists Conference, Honolulu, Hawaii, USA 2010

[18] V. Quasching, R. Hanitsch, Sol. Energy 56 (6) (1996) 513.